# Case History and Analysis of the Spiral Vibration of a Large Turbogenerator Using Three Different Heat Input Models

**Lothar Eckert**
Turbogenerator R&D
ALSTOM (Switzerland) Ltd
CH-5242 Birr, Switzerland
lothar.eckert@power.alstom.com

**Joachim Schmied**

DELTA JS AG
CH-8005 Zurich, Switzerland
jschmied@delta-js.ch

**Alfred Ziegler**
Turbogenerator R&D
ALSTOM (Switzerland) Ltd
CH-5242 Birr, Switzerland
alfred.ziegler@power.alstom.com

## ABSTRACT

The phenomenon of spiral vibration (Newkirk-effect) may be observed in various types of rotating machinery. It is caused by a vibration-induced hot spot on the shaft surface, which is generated by friction. Spiral vibration with a forward rotating unbalance vector occurred at a hydrogen-cooled turbogenerator. From tests with the running generator the carbon brushes sliding on the slip rings were identified as the hot spot location. Potential modifications were studied using hot spot stability analyses with a rotor dynamic model of the generator shaft. The applied method, introduced by Schmied, allows the handling of general systems. It uses a hot spot model based on Kellenberger's thermal equation between the shaft's thermal deflection and its displacement. In the case of slip rings, the hot spot is caused by friction from the carbon brushes. The stability threshold is determined as a function of rotor speed and the ratio of added to dissipated heat. Three different relations between the added heat and the shaft vibration were modelled: heat input proportional to the shaft displacement, to the shaft velocity and to the shaft acceleration. The model with the heat input proportional to the velocity was found to be the most suitable variant. This was confirmed by comparison with measurements. Finally, a modification was selected based on the calculation results and successfully implemented.

## KEY WORDS

Newkirk-effect, rotating unbalance vector, vector turning, hot spot phenomenon, stability analysis

## 1  INTRODUCTION

Spiral vibration is a phenomenon that is observed in various types of rotating machinery, e.g. compressors, water turbines, steam turbines and turbogenerators. It is caused by a vibration-induced hot spot on the shaft surface generated by friction due to "soft" rubbing of the shaft to stationary (non-rotating) parts, e.g. labyrinth seals, seal rings, oil film of journal bearings, hydrogen seals or brushes on slip rings.

Spiral vibration is characterized by sinusoidal variation in amplitude versus time plots (Figure 1) or by circular loops of the measured unbalance response vector on a polar plot (Figure 2). The phenomenon is also referred to as Newkirk- [11] or Morton-effect [2], [3], [4] and [8], rotating vectors or vector turning [1]. Various rub-related phenomena are described in the literature survey of M. Muszynska [10].
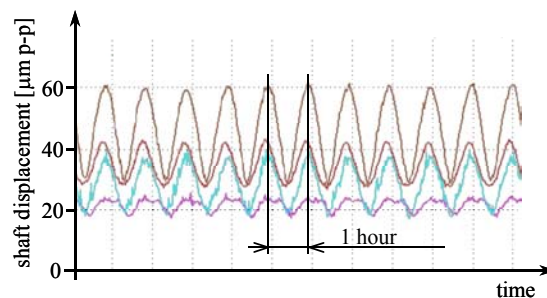


**Figure 1:** Amplitude versus time plot in case of spiral vibration. Period: 1 h.
Sinusoidal curve of relative shaft vibration at various bearings of a steam turbine generator set

An increasing magnitude of the spiral, which does not end in a limit cycle leads to an unacceptable high level of vibration and enforces a shutdown of the machine. Spiral vibration on a limit cycle with acceptable amplitude is satisfactory if the cause of the spiral vibration is known and is of no concern for any machine component. The rotation of the unbalance vector is slow with periods $T$ for one 360°-turn of the vector between 20 mins and several hours (Table 1). On turbogenerators both rotation directions were observed: backward and forward rotation of the unbalance response vector. The classic case of a backward rotating vector due to heat input proportional to the shaft displacement is well described in textbooks [1] and [5]. The forward rotating vector is explained with a simplified two degrees of freedom system in [1] by inertia modulated heat input proportional to the shaft acceleration.

This paper describes the case history of a 450 MVA, 3600 rpm hydrogen-cooled turbogenerator equipped with a brush gear unit, which showed the phenomenon of spiral vibration with a forward rotating unbalance vector. This case could only be described with a model where the heat input was proportional to the shaft velocity. According to the authors' knowledge this case was not yet studied in literature. The root cause analysis, the hot spot stability analyses using three different heat input models and finally the successful modification are described further below.

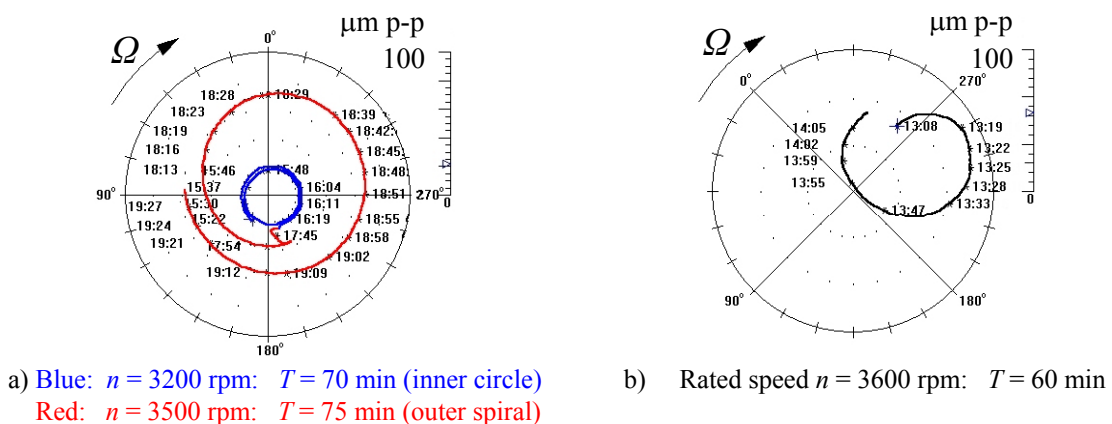**Table 1:** Cases of spiral vibration at turbogenerators

| Power in MW or MVA | Speed (rpm) | Rotation direction of vector (2) | Period $T$ for 360°-turn | Ref. | Author |
|---|---|---|---|---|---|
| 100 MW | 3000 | (-) backward | 20 min | [6] | Kellenberger |
| 650 MW | 3600 | (-) backward | 3.5 h | | |
| 722 MVA | 3600 | (-) backward | 3.2 h | [7] | Kellenberger |
| 600 MVA | 3000 | (-) backward | not given | [12] | Schmied |
| 760 MW | 3600 | (+) forward | 3 h | [1] | Adams |
| 450 MVA | 3600 | (+) forward | 1 h | this paper | Eckert et al. |
| 1180 MVA | 3000 | (-) backward | 70 – 100 min | this paper | Eckert et al. |
| 1180 MVA | 2350 (1) | (+) forward | | | |
| (1): below rated speed of 3000 rpm | | (2): (-): backward (counter-rotational) (+): forward (co-rotational) | | | |

## 2 ROOT CAUSE ANALYSIS

Prior to release of turbogenerator up rates, the machine is tested to verify all electrical and performance data. The turbogenerator is mounted on a test stand in the factory and driven by a synchronous motor. The generator is operated at its rated speed. The drive motor only needs to deliver the losses of the generator (around one per cent of the machine's rated power).

During the running test of a hydrogen-cooled turbogenerator with three bearings spiral vibration with increasing magnitude occurred. In the text below the three bearings will be referred to as DE- (driven end), NDE- (non-driven end) and end bearing (Figure 6). Spiral vibration with increasing magnitude would limit the duration of continuous running in the power plant. Immediately a root cause analysis was started to solve the problem. Various tests with the running generator were performed with the aim to identify the location of the hot spot. In parallel a hot spot calculation model was set up.

### 2.1 Measured vibrational behaviour



a) Blue:  $n = 3200$ rpm:  $T = 70$ min (inner circle)     b)   Rated speed $n = 3600$ rpm:  $T = 60$ min
   Red:  $n = 3500$ rpm:  $T = 75$ min (outer spiral)

**Figure 2:** Polar plots of measured vibration at different rotor speeds $n$ and period $T$ for one 360°-turn.
   a) Horizontal DE-bearing pedestal vibration    b) Relative shaft vibration at NDE-bearing

The generator was run at speeds below rated speed in order to find out the speed range during which the spiral vibration occurs. Figure 2 shows the measured vibrations for the speeds 3200, 3500 and 3600 rpm. At 3200 rpm the magnitude of the spiral was stable and the spiral became a limit circle. Above 3200 rpm the spiral vibration has increasing magnitude in a wide speed range of more than 400 rpm. At all three speeds a forward rotating vector was observed.

## 2.2  Potential hot spot locations

The vibration-induced hot spots may be generated at various locations of hydrogen-cooled turbogenerators, such as:

1. Labyrinth seals at the hydrogen seals, bearing pedestals and the brush gear housing
2. Oil film in journal bearings
3. Seal ring of the hydrogen seals and
4. Carbon brushes sliding on the two slip rings.

The labyrinth seals were excluded by inspection of the clearances. The journal bearings and the hydrogen seal ring were excluded by variation of the lube oil temperatures and lube oil flows, which did not change the vibrational behaviour. A test without carbon brushes revealed that the carbon brushes sliding on the slip rings were the location of the hot spot. The generator was brought to rated speed without brushes and operated for about one hour. No spiral vibration occurred. Immediately after insertion of the brushes, which can be done under operational conditions, spiral vibration appeared with increasing magnitude. After brush removal the spiral vibration promptly stopped and the vibration vector returned straight to its original position, when the test was started. Figure 3 shows the polar plot of the relative shaft vibration measured at the NDE-bearing during this run.
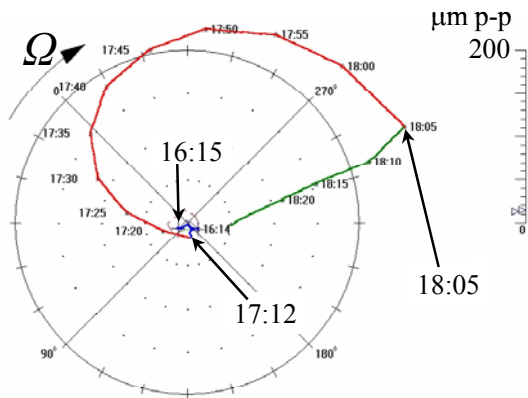


16:15 – 17:12:
Run at rated speed of 3600 rpm without brushes
→ Stable vibration amplitude.
17:12:  Brushes installed
→ Spiral vibration started (red line)
18:05:  Brushes removed
→ Spiral vibration stopped (green line)

**Figure 3:**  Measured relative shaft vibration at NDE-bearing. Rotor speed $n$ = 3600 rpm

## 2.3  Brush Gear and Carbon Brushes

The brush gear unit supplies the DC-current to the field winding of the generator rotor. The field current of hydrogen-cooled generators is in the range from 3000 to 7000 A. The slip ring shaft (SR) with two slip rings and a radial fan for cooling is supported by the NDE- and the end bearing. Carbon brushes sliding on the slip rings transfer the current from the stationary brush holders (Figure 4) to the rotating slip rings. The slip rings are shrunk on the shaft via soft insulation material for electrical insulation. Nevertheless the thermal bow of the slip rings is transmitted to the shaft to some extent. Slip ring shafts may be particularly prone to the spiral vibration phenomenon due to the friction heat that is inevitably generated by the brushes. During operation the generated friction heat may increase due to too low humidity (below 4.5 gr/m$^3$ H$_2$O abs.) or too low current density (below 5.5 to 8 A/cm$^2$).

## 3  HOT SPOT STABILITY ANALYSIS

With a hot spot stability analysis using a rotor dynamic model of the generator rotor potential modifications were studied. The modelling of the hot spot phenomenon is based on the theory of Kellenberger [6] and [7] using a thermal equation between the shaft's thermal deflection and the shaft displacement at the location of a hot spot. In case of slip rings, the friction between brushes and shaft causes the hot spot. The contact forces of the brushes around the circumference may vary due to the shaft vibration and cause a thermal bend of the slip ring shaft due to the differential heat input. The stability threshold is determined as a function of the rotor speed and the ratio of the added heat to the dissipated heat at the slip rings. A threshold at low ratio indicates that the shaft is sensitive to hot spots, i.e. little heat input is necessary to destabilise the system.

The calculation method for generalised shaft systems according to Schmied [12] is applied for three different relations between the heat input and the shaft vibration (see section 3.2).

## 3.1 Calculation Method

The equation of motion of the Finite Element model of a multi bearing turbine generator set has the form:

$$\mathbf{M}\ddot{\mathbf{x}} + (\mathbf{D} + \mathbf{G})\dot{\mathbf{x}} + \mathbf{Kx} = \mathbf{f}(t) \tag{1}$$

with the mass matrix $\mathbf{M}$, the damping matrix $\mathbf{D}$, the gyroscopic matrix $\mathbf{G}$ and the stiffness matrix $\mathbf{K}$.

The matrices $\mathbf{D}$ and $\mathbf{K}$ are non-symmetric due to the damping and stiffness coefficients of the journal bearing and dependant on rotor speed.

If the rotor is thermally deformed the equation of motion for coordinates $\mathbf{x}$ relative to the static position of the rotor not deformed is

$$\mathbf{M}\ddot{\mathbf{x}} + (\mathbf{D} + \mathbf{G})\dot{\mathbf{x}} + \mathbf{Kx} - \mathbf{K}^\mathbf{R}\mathbf{x_T} = \mathbf{f}(t) \quad , \tag{2}$$

where $\mathbf{K}^\mathbf{R}$ is the stiffness matrix of the rotor alone (without pedestals and journal bearings) and $\mathbf{x_T}$ is the vector describing the thermal deformation.

The thermal deformation $\mathbf{x_T}$ is assumed to depend linearly on the thermal deflections $\mathbf{x_{T,HS}}$ of the shaft at the location of the hot spot (HS):

$$\mathbf{x_T} = \mathbf{T}\,\mathbf{x_{T,HS}} \tag{3}$$

$$\mathbf{x_{T,HS}} = \left( x_{T,h}, \, x_{T,v} \right)^\mathbf{T} \tag{4}$$

where $\mathbf{x_{T,h}}$ and $\mathbf{x_{T,v}}$ are the thermal translatory deflections in horizontal and vertical direction at the location of the hot spot. The matrix $\mathbf{T}$ is derived from the thermal deformation of the rotor (see Figure 7), which is determined by a static calculation with thermal loads: for the first column of $\mathbf{T}$ for a temperature gradient in horizontal direction and for the second column for a temperature gradient in vertical direction.

## 3.2 Three Different Heat Input Models

The modelling of the hot spot phenomenon according to the theory of Kellenberger is based on the following thermal equation:

$$\dot{\tilde{\mathbf{x}}}_{\mathbf{T,HS}} = \underbrace{p\Omega\,\tilde{\mathbf{x}}_{\mathbf{HS}}}_{\dot{\mathbf{Q}}^+} - \underbrace{q\,\tilde{\mathbf{x}}_{\mathbf{T,HS}}}_{\dot{\mathbf{Q}}^-} \tag{5a}$$

with $\tilde{\mathbf{x}}_{\mathbf{T,HS}}$ as the thermal deflection at the location of a hot spot and

$\tilde{\mathbf{x}}_{\mathbf{HS}} = \left( \tilde{x}_h, \, \tilde{x}_v \right)^T$ as the vector of the translatory shaft displacements at the location of the hot spot.

$\dot{\mathbf{Q}}^+$ is the added heating efficiency and $\dot{\mathbf{Q}}^-$ is the dissipated heating efficiency.

Equation (5a) was derived in detail by Kellerberger (see [6], [7]). The coordinates in Eq. (5a) are rotating in contrast to the coordinates in Eqs. (1), (2) and (3) which are stationary (Figure 5).

Equation (5a) implies the following:
- The change of cross sectional temperature difference is proportional to the change of thermal deflection,
- The differential heat input across the shaft cross section is proportional to the shaft displacement and the speed,
- The differential dissipated heat across the shaft cross section is proportional to the thermal deflection.

The proportionality factors for the added and dissipated heat are $p$ and $q$. Kellenberger has applied the method to simplified shaft models. The method was extended for the use on general shaft systems – see [12].

In Eq. (5a) the heat input is proportional to the deflection of the shaft at the location of the hot spot. This is a good approximation for the effect in a journal bearing or labyrinth seals.

However in case of slip rings, the hot spot is caused by the friction between the carbon brushes and the slip ring. The brushes are pressed against the slip ring by roller springs (Figure 4). The pressure around the circumference may vary due to the shaft vibration. In case of a synchronous vibration it is always the same point on the shaft, which is submitted to an increased heat input. The pressure can vary due to the following three mechanisms (Figure 5, case a to c). The brush contact force varies:

a) Due to the stiffness of the roller springs,
b) Due to the friction in the brush holder, which inhibits the movement of the brush in radial direction,
c) Due to the inertia effects of the brushes.

Case a: The original thermal Equation (5a) can be applied. However, the roller springs are designed to provide a constant force not dependent on spring displacement or brush wear respectively and thus have very low spring stiffness. Therefore, it is highly likely, that one of the other two mechanisms prevails.

Case b: It is assumed that the heat input is proportional to the shaft velocity instead of the shaft displacement, since a friction force changes its direction with the direction of the velocity. This yields the following thermal equation (5b):

$$\dot{\widetilde{\mathbf{x}}}_{\mathbf{T,HS}} = p\Omega\,\dot{\widetilde{\mathbf{x}}}_{\mathbf{HS}} - q\,\widetilde{\mathbf{x}}_{\mathbf{T,HS}} \tag{5b}$$
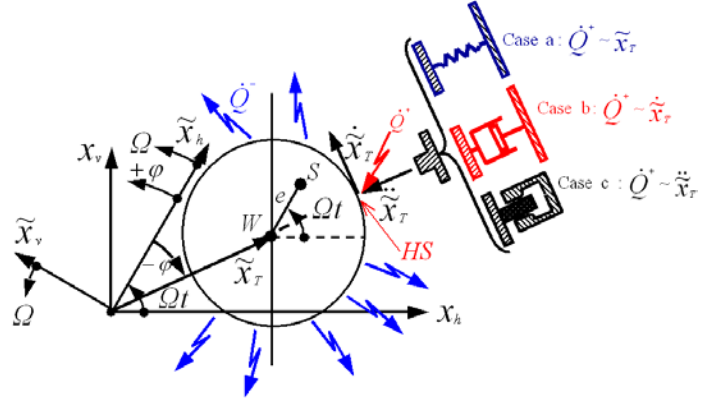
Case c: The heat input is assumed to be proportional to the shaft acceleration, i.e. the following thermal equation applies:

$$\dot{\widetilde{\mathbf{x}}}_{\mathbf{T,HS}} = p\Omega\,\ddot{\widetilde{\mathbf{x}}}_{\mathbf{HS}} - q\,\widetilde{\mathbf{x}}_{\mathbf{T,HS}} \tag{5c}$$

The most suitable case will be selected by comparison of the analytical results to the practical experience (see section 4.4).
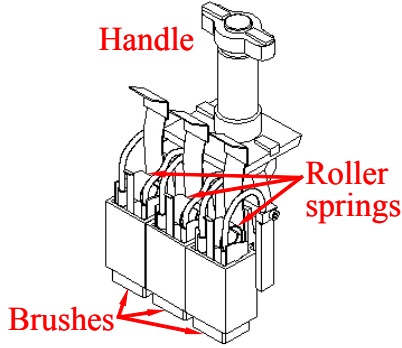


**Figure 4:** Brush carrier holding three brushes    **Figure 5:** Three heat input mechanisms of brushes

### 3.3  Hot Spot Stability, Thermal Eigenvalues

Transforming Equation (5a) into stationary coordinates $x_{T,h}$, $x_{T,v}$, $x_h$, $x_v$ yields:

$$\begin{bmatrix} 1 & 0 \\ 0 & 1 \end{bmatrix}\begin{bmatrix} \dot{x}_{T,h} \\ \dot{x}_{T,v} \end{bmatrix} + \begin{bmatrix} -p\Omega & 0 \\ 0 & -p\Omega \end{bmatrix}\begin{bmatrix} x_h \\ x_v \end{bmatrix} + \begin{bmatrix} q & \Omega \\ -\Omega & q \end{bmatrix}\begin{bmatrix} x_{T,h} \\ x_{T,v} \end{bmatrix} = \begin{bmatrix} 0 \\ 0 \end{bmatrix} \tag{6}$$

Or by using matrices and vectors

$$\mathbf{I}\,\dot{\mathbf{x}}_{\mathbf{T,HS}} + \mathbf{P}\,\mathbf{x}_{\mathbf{HS}} + \mathbf{Q}\,\mathbf{x}_{\mathbf{T,HS}} = \mathbf{0} \tag{7}$$

Substituting (3) into (2) and extending (2) by (7) yields

$$\underbrace{\begin{bmatrix} \mathbf{M} & \mathbf{0} \\ \mathbf{0} & \mathbf{0} \end{bmatrix}}_{\mathbf{A}}\begin{bmatrix} \ddot{\mathbf{x}} \\ \ddot{\mathbf{x}}_{\mathbf{T,HS}} \end{bmatrix} + \underbrace{\begin{bmatrix} (\mathbf{D}+\mathbf{G}) & \mathbf{0} \\ \mathbf{0} & \mathbf{I} \end{bmatrix}}_{\mathbf{B}}\begin{bmatrix} \dot{\mathbf{x}} \\ \dot{\mathbf{x}}_{\mathbf{T,HS}} \end{bmatrix} + \underbrace{\begin{bmatrix} \mathbf{K} & -\mathbf{K_R T} \\ \mathbf{P} & \mathbf{Q} \end{bmatrix}}_{\mathbf{C}}\begin{bmatrix} \mathbf{x} \\ \mathbf{x}_{\mathbf{T,HS}} \end{bmatrix} = \begin{bmatrix} \mathbf{0} \\ \mathbf{0} \end{bmatrix}\quad, \tag{8}$$

where $\mathbf{P}$ is a 2 x $N$ matrix (with $N$ as the dimension of Eq. (2)), which has the coefficients of $\mathbf{P}$ at the columns of the translatory coordinates $\mathbf{x}_{\mathbf{HS}}$ of the hot spot. Equation (8) is valid for the heat input proportional to the shaft displacement according Eq. (5a). For the other two models with heat input proportional to shaft velocity (Eq. (5b)) and shaft acceleration (Eq. (5c)) respectively, the parameter matrix $\mathbf{P}$ appears in matrix $\mathbf{B}$ and $\mathbf{A}$ respectively, instead of $\mathbf{C}$.

To receive Equation (8) the original Finite Element model of the rotor represented by Equation (1) must be extended by introducing the two extra degrees of freedom $x_{T,h}$ and $x_{T,v}$. The additional coefficients must be added to the global matrices. This possibility is provided for the input of the program MADYN [9].

From Equation (8) one could calculate the time history of $\mathbf{x}$ by a time step method. The polar plot of the time history of each coordinate would be a spiral either increasing or decreasing in magnitude. This calculation however, would require larger computational effort, since the period of a spiral to complete a 360°-turn is very long for realistic examples (see Table 1). That is why the computation would require the simulation of quite a long period of time until one could judge whether a spiral increases or decreases in magnitude.

As described in [12] this information could be easier extracted from the complex eigenvalues of Equation (8). Their calculation requires little computational effort.

Equation (8) has 2(N+1) eigenvalues. Since realistic values for $p$ and $q$ are very small - $p$ is in the order of magnitude of $10^{-4}$ and $q$ is in the range of $10^{-3}\omega_0$ where $\omega_0$ is a representative natural frequency of the rotor system (see [6] and [12]) - a set of 2N eigenvalues are practically the same as those of Equation (1) representing the rotor system.

The additional two eigenvalues are a conjugate complex pair:

$$\lambda_T = \alpha \pm i\nu \tag{9}$$

and will be called "thermal" eigenvalue in the following. The imaginary part $\nu$ of the thermal eigenvalue is almost equal to $\Omega$. The interpretation of the thermal eigenvector (so-called hot spot mode) is derived in [12]:

The difference between $\nu$ and $\Omega$ indicates how fast the thermal bow moves along the shaft respectively at which speed the spiral is traced. The period to complete 360°-turn of the spiral is:

$$T = 2\pi / |\nu - \Omega| \qquad (10)$$

The direction of the revolution of the unbalance response vector is as follows:

$\nu > \Omega$   Forward   (co-rotational, same direction as the rotor spin)
$\nu < \Omega$   Backward (counter- rotational, opposite direction as the rotor spin).   (11)

The real part of the thermal eigenvalue $\lambda_T$ indicates whether the spiral increases or decreases in magnitude:

$\alpha > 0$   Increasing magnitude (unstable behaviour)
$\alpha < 0$   Decreasing magnitude (stable behaviour).   (12)

## 4  CALCULATION RESULTS

### 4.1  Rotor Model

The model of the turbogenerator with brush gear unit consists of the generator rotor (GEN) and the slip ring shaft (SR), supported on three journal bearings in free-standing pedestals, which are modelled as equivalent mass-spring-damper systems with representative parameters for the horizontal and vertical direction. In Figure 6 the location of the slip rings 1 and 2 and the three bearings (DE-, NDE- and end-bearing) are indicated.

The thermal deformations of the shaft for a temperature difference of 1°K across the section over the seat length of slip ring 1 are shown in Figure 7. The maximum deflection occurs at slip ring 1 with 2.8 μm/°K in horizontal direction and with 2.9 μm/°K in vertical direction. For the temperature difference at slip ring 2 the maximum defection are 3.2 μm/°K in horizontal direction and 3.3 μm/°K in vertical direction, respectively.
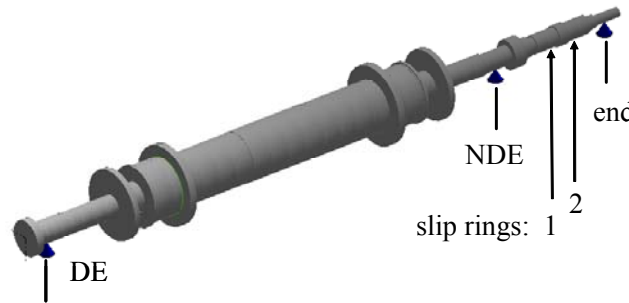


**Figure 6:** Rotor model of the turbogenerator with slip ring shaft between the NDE- and the end bearing



a)                                                                    b)
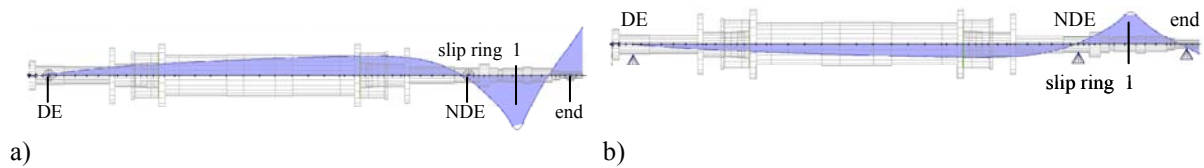
**Figure 7:** Thermal defection due to hot spot at slip ring 1.  a): horizontal deflection,   b): vertical deflection

### 4.2  Campbell Diagrams

The generator rotor has four critical speeds $n_k$ up to rated speed of 3600 rpm (Table 2).

**Table 2:**  Natural frequencies and damping ratios at rated speed (6 modes)

| | | k=1 | k=2 | k=3 | k=4 | k=5 | k=8 |
|---|---|---|---|---|---|---|---|
| | | GEN - 1st bending | GEN - 1st bending | GEN - 2nd bending | GEN - 2nd bending | SR - 1st bending | SR - 1st bending |
| | | horizontal | vertical | horizontal | vertical | horizontal | vertical |
| k-th natural frequency $f_k$ | Hz | 9.99 | 10.75 | 26.57 | 30.02 | 55.19 | 82.35 |
| k-th natural frequency $f_k$ | cpm | 600 | 650 | 1590 | 1800 | 3310 | 4940 |
| modal damping ratio $D_k$ | % | 0.5 | 0.3 | 3.8 | 0.2 | 15.4 | 2.5 |

The 1st bending modes of the generator (GEN) and the slip ring shaft (SR) have U-shape. The 2nd bending modes of the GEN-rotor have S-shape. Table 2 summarizes the natural frequencies and corresponding damping ratios at rated speed.

The natural frequencies of the generator (k=1 to 4) are well below rated speed and have minor influence on the hot spot stability. The modes with largest influence on the hot spot behaviour are the two slip ring shaft modes (SR 1st bending horizontal / vertical) shown in Figure 8. For these two SR-modes the natural frequency and damping ratio as functions of speed are plotted in a Campbell diagram (Figure 10 a, original design). The rated speed is between the critical speeds of the horizontal and vertical slip ring shaft mode. The natural frequency of the horizontal SR-mode (3310 cpm) is close to rated speed. This mode is highly damped, with a damping ratio of about 20% at its critical speed.

a)                                                                 b)
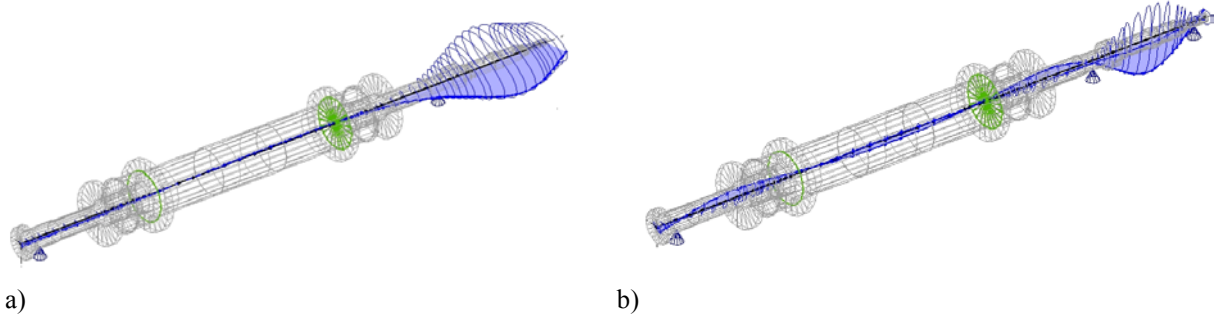
**Figure 8:** Slip ring shaft (SR)-modes at rated speed.   a): horizontal,   b): vertical
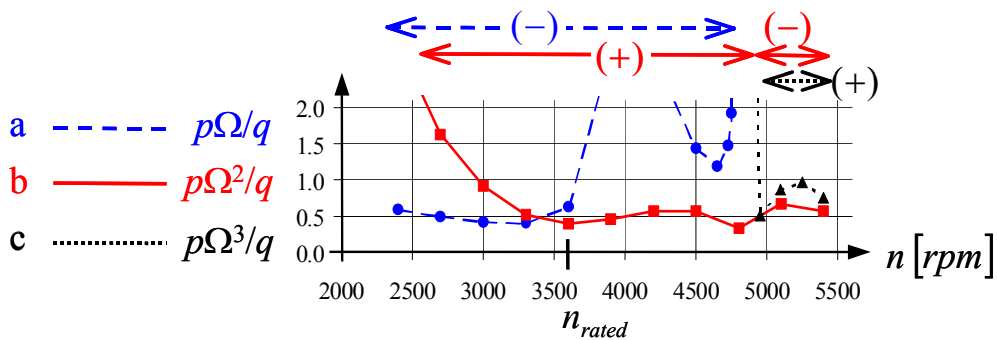
### 4.3 Hot Spot Stability Charts

The analysis as described yields additional natural modes – the hot spot modes. The hot spot modes are the rotor response to the thermal bent shaft, basically an unbalance response.

The assessment of the hot spot stability is carried out in two steps:

1. Determination of the threshold as ratio of the added to dissipated heat at the slip rings as a function of the rotor speed: For heat input below the threshold the vibration amplitude decays to a value corresponding to the residual unbalance; in case it is above the threshold the vibration amplitude theoretically increases to infinity. Practically it will stabilise at a high level due to non-linearity, which is not considered in the model. The stability threshold primarily is a property of the rotor bearing system and its natural modes respectively.

2. Estimation of the ratio p/q for the added to dissipated heat as done in [12] for heat input proportional to shaft displacement in a journal bearing and heat input proportional to shaft acceleration for brushes on slip rings: The analytical estimation is done with two assumptions: 1. The thermal bow of the slip ring is fully transmitted to the shaft. 2. The orbit at the slip rings is circular with 10 μm s.a. = 20 μm p-p. The first assumption is probably to extreme due to the soft insulation material between the slip rings and the shaft.

Figure 9 shows the stability charts for the three different heat input models described in section 3.2. The dimensionless heat ratios for the case b and c are $p\Omega^2/q$ and $p\Omega^3/q$, respectively. The "±"-signs indicate the direction of the unbalance vector turning due to the hot spot: "(+)" for forward (co-rotational) and "(-)" for backward (counter-rotational). For case b the estimated ratio $p\Omega^2/q$ for the added to dissipated heat at rated speed is 6.64 for an orbit of 20 μm p-p and lies far above the stability threshold in the unstable region. The ratio decreases with increasing vibration level due to non-linear friction and thus stabilises at a high vibration level.

a : heat input ~ shaft displacement        b :  heat input ~ shaft velocity        c :  heat input ~ shaft acceleration

**Figure 9:**  Stability charts for the three different heat input models. Case a, b and c

Since the model has two hot spot locations two "thermal" modes appear. One thermal mode is a kind of 1st bending of the slip ring shaft (temperature differences in phase), the 2nd mode a kind of 2nd bending (temperature differences out of phase). The 2nd thermal mode has the higher stability threshold, i.e. the stability is determined by the 1st mode. In case of the acceleration heat input model the 2nd thermal mode is always stable, no threshold exists for this mode. One would have obtained similar results using only one hot spot location for the two slip rings.

The shape of the stability threshold lines are mainly determined by the horizontal and vertical SR-resonances:

Case a (Figure 9, blue): For the displacement heat input model the threshold is low in the whole speed range below the horizontal SR-resonance (3300 rpm). Above this resonance the threshold increases steeply. Close to the vertical SR-resonance only a small spike with lower threshold appears. Only backward rotating vectors (-) occur in the whole speed range.

Case b (Figure 9, red): For the velocity model the threshold decreases from low speeds towards the horizontal SR-resonance and than remains at low level for higher speeds. A forward rotating vector (+) occurs below 4950 rpm (vertical SR-resonance) and backward (-) above 4950 rpm.

Case c (Figure 9, black): The acceleration model is unstable above the vertical SR-resonance (4950 rpm) with a forward rotating vector (+) only.

This behaviour can be explained with the simplified two degrees of freedom system used by Adams [1] by the phase angle φ of the response to an unbalance or thermal bending of the slip ring shaft. In case of a small angle φ, i.e. in the sub critical region, the displacement model yields a heat input in the same direction as an unbalance and thus can amplify an initial thermal bending (→ low threshold). For the velocity model this situation occurs for a phase angle φ around -90°, since the velocity is 90° ahead of the displacement. For the acceleration model this situation occurs only in the supercritical region with phase angle between -90° and -180°). Thus the six cases given in Table 3 may be distinguished.

**Table 3:** Six Cases of Vibration Induced Hot Spot Spiral Vibration (inspired by Adams [1], case 1 to 4)

| Rotor speed Ω, phase angle φ between response and thermal unbalance | Heat input ~ shaft displacement | Heat input ~ shaft velocity | Heat input ~ shaft acceleration |
|---|---|---|---|
| Sub critical:  Ω < ω$_k$ | | | |
| -90° < φ < 0,  case 1 and 3 in [1] | Backward (-) Rotation. Increasing magnitude, Spiralling likely | | Forward (+) Rotation. Decreasing magnitude, No Spiralling |
| -90° φ < -45 | | Forward (+) Rotation. Increasing magnitude, Spiralling likely | |
| Supercritical:  Ω > ω$_k$ | | | |
| -180° < φ < -90°  case 2 and 4 in [1] | Backward (-) Rotation. Decreasing magnitude, No Spiralling | | Forward (+) Rotation. Increasing magnitude, Spiralling likely |
| -135° < φ < -90° | | Backward (-) Rotation. Increasing magnitude, Spiralling likely | |

## 4.4 Selection of the Adequate Heat Input Model

As shown in Figure 2 only the forward rotating vector was observed in the speed range from 3200 rpm to 3600 rpm. With the acceleration model (case c) no unstable behaviour was calculated at 3600 rpm below the vertical SR-resonance. The displacement model (case a) does not show a forward rotating vector at 3600 rpm, and at speeds below the vertical SR-resonance, respectively. This model is also questionable due to the design of the springs in the brush holder. Roller springs have very low stiffness.

Only the hot spot modes calculated for case b with the heat input proportional to the shaft velocity matches the observed spiral vibration behaviour with forward rotating vector. The stability threshold of case b is low enough at rated speed to explain the increasing magnitude due to the hot spot phenomenon. Therefore, the case b model is used to investigate potential modifications.

The calculated behaviour of case b matches also the case of an 1180 MVA, 3000 rpm turbogenerator (Table 1), which showed spiral vibration with a backward rotating vector at 3000 rpm, a forward rotating vector at 2350 rpm and no spiral vibration at 3200 rpm. The slip ring shaft critical speed with 2830 rpm was initially too close to rated speed and was shifted to lower speeds by increasing the bearing span of the slip ring shaft to solve the problem.

## 4.5 Potential Modifications and Selected Modification

The following options were considered:
1. Use of carbon brushes with low friction coefficient (of 0.14 instead of 0.26 for standard brush),
2. Shift the horizontal SR-critical speed above rated speed by increased horizontal stiffness of the journal bearings using other journal bearing types,

3. Shift both – the horizontal and vertical - SR-critical speed below rated speed by increasing the bearing span between the NDE- to end-bearing.

The use of low friction brushes (option 1) will reduce the vibration level through the reduction in heat input, however this will not eliminate the sensitivity of the shaft line to spiral vibration behaviour. Option 2 is promising, because the horizontal SR mode has the main influence on the hot spot behaviour. It was studied together with option 3 by calculating Campbell diagrams and hot spot stability charts.

Option 3 would require an increase of the bearing span by more than one meter and a large effort to implement within the power plant. With option 2 finally an appropriate bearing configuration was found to shift the horizontal SR-mode well above rated speed. This bearing modification was selected to overcome the spiral vibration with increasing magnitude. The modification consists of five tilting-pad bearings ("load between pads") at both – the NDE- and end-bearing.

Figure 10 compares the natural frequency $n_k$ and damping ratio $D_k$ of horizontal SR-mode of the original and the modified bearing configuration. In Figure 11 the calculated hot spot stability charts of the original and the proposed modification are shown. The hot spot stability chart of the modified configuration clearly shows that the unstable region is shifted to higher rotor speeds as the horizontal slip ring shaft mode is shifted to higher frequencies. Note the higher heat ratio at the stability threshold at 3600 rpm: The vibration level is expected to drop to less than 30% of the original value.



a) Original design     b) Selected Modification: Five-tilting-pad bearings at NDE- and end bearing
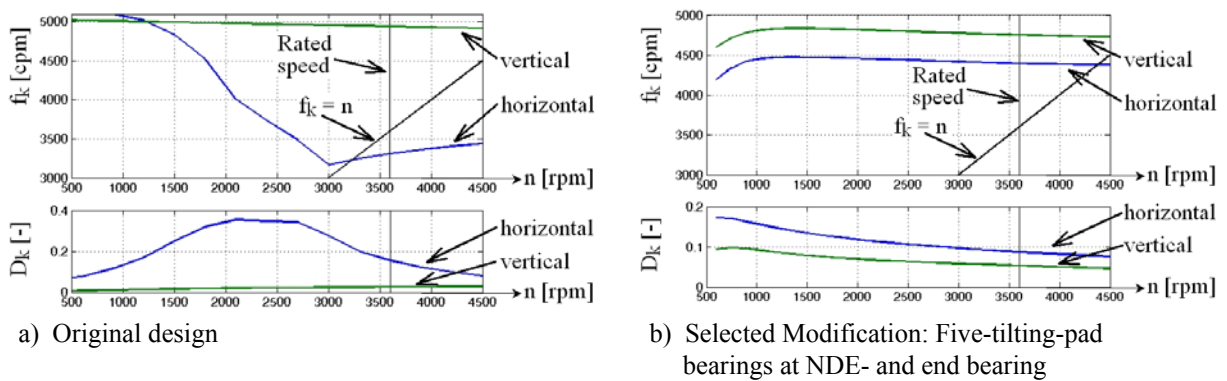
**Figure 10:** Campbell diagram of horizontal and vertical slip ring shaft mode



a ——— before modification $p\Omega^2/q$
b - - - - - after modification
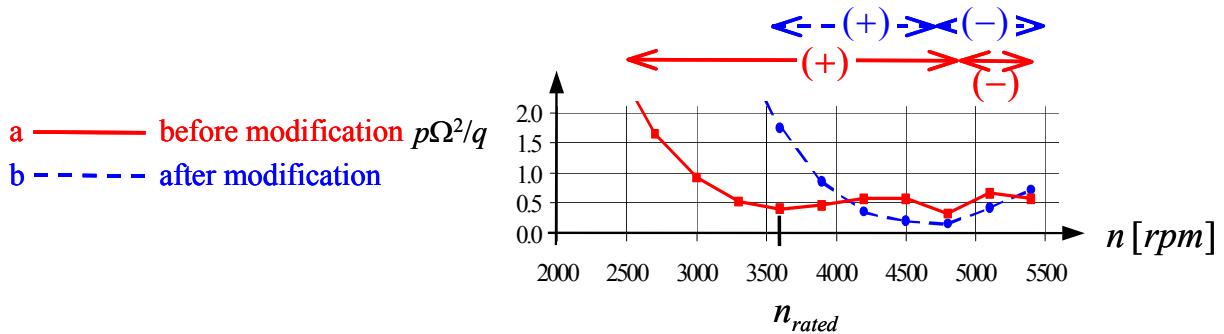
**Figure 11:** Hot spot stability chart before and after modification. Heat input proportional to shaft velocity

## 5  MODIFICATION ON SITE

During the initial commissioning in the power plant low friction brushes were used to reduce the vibration levels. They were replaced by standard brushes when five tilting-pad bearings were installed at the NDE- and end bearing of the turbogenerator.

With the bearing modification the spiral vibration is reduced to small magnitude even with higher friction. Figure 12 shows the measured relative shaft vibration at the NDE-bearing before and after the modification.



a) before modification          b) after modification
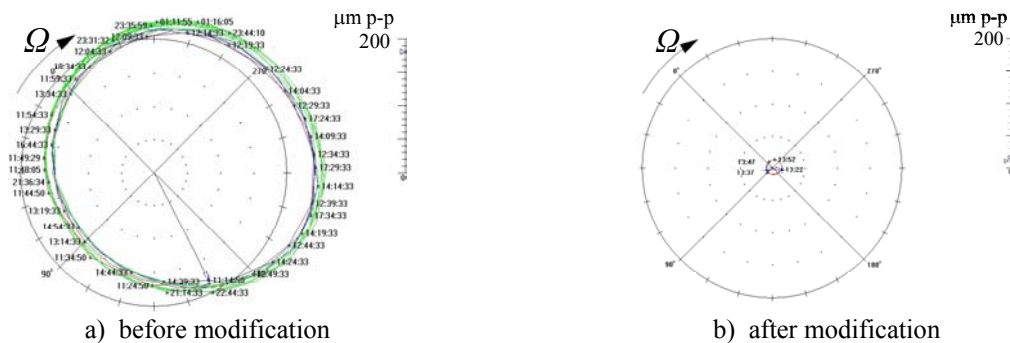
**Figure 12:** Polar plot of measured relative shaft vibration at NDE-bearing

## 6  CONCLUSION

A 450 MVA, 3600 rpm hydrogen-cooled turbogenerator equipped with a brush gear unit showed the phenomenon of spiral vibration with a forward rotating vector. After tests with the running turbogenerator the carbon brushes sliding on the slip rings were identified as the hot spot location.

With the help of hot spot stability analyses using a rotor dynamic model of the generator rotor on three bearings potential modifications were studied. In the case of slip rings, the friction between brushes and shaft causes the hot spot. The stability threshold is determined as a function of the rotor speed and the ratio of the added heat to the dissipated heat at the slip rings. A threshold at low ratio indicates that the shaft is sensitive to hot spots, i.e. little heat input is necessary to destabilise the system. Three different relations between the heat input and the shaft vibration were modelled: heat input proportional to the shaft displacement, to the shaft velocity and to the shaft acceleration. The model, in which the heat input is proportional to the velocity was found to be the most suitable variant for brushes on slip rings, which was confirmed by comparison with the measured vibration. Finally, a modification of the generator shaft line was selected based on the calculation results: both slip ring shaft critical speeds were shifted well above rated speed by using five tilting-pad bearings at the NDE- and end bearing. The modification was successfully implemented within the power plant.

## ACKNOWLEDGEMENT

## REFERENCES

[1]    Adams, Maurice L. (2001): *Rotating Machinery Vibration from Analysis to Troubleshooting*. Marcel Dekker, Inc. New York, Basel 2001, chapter 12.3 "Vector Turning from Synchronously Modulated Rubs", pp. 312-318

[2]    Balbahadur, Avinash C. (2001): *A Thermoelastohydrodynamic Model of the Morton Effect Operating in Overhung Rotors Supported by Plain or Tilting Pad Journal Bearings*. Ph.D. Dissertation, Faculty of the Virginia Polytechnic Institute and State University, Blacksburg, Virginia, 2001

[3]    Balbahadur, Avinash C., Kirk; R. G.(2004): Part I—Theoretical Model for a Synchronous. Thermal Instability Operating in Overhung Rotors. *International Journal of Rotating Machinery*, 10(6): 469–475, 2004

[4]    De Jongh, F. M., Morton, P. G. (1996): The synchronous instability of a compressor rotor due to bearing journal differential heating. *Journal of Engineering for Gas Turbines and Power*, October 1996, Vol. 118, pp. 816-824

[5]    Gasch, R., Nordmann, R., Pfützer, H. (2002): *Rotordynamik*. 2. vollständig neu bearbeitete und erweiterte Auflage, Springer-Verlag 2002, Kapitel 26 "Der sanft anstreifende Rotor", pp. 537-554

[6]    Kellenberger, W. (1978): Das Streifen einer rotierenden Welle an einem federnden Hindernis - Spiralschwingungen. *Ingenieur-Archiv*, Nr. 47 (1978), pp. 223-229

[7]    Kellenberger, W. (1980): Spiral Vibrations Due to the Seal Rings in Turbogenerators Thermally Induced Interaction Between Rotor and Stator. *Journal of Mechanical Design*, January 1980, Vol. 102, 177-184

[8]    Keogh, P. S., Morton, P.G. (1993): Journal Bearing Differential Heating Evaluation With Influence on Rotor Dynamic Behaviour. *Proceedings of the Royal Society*, London, Vol. A441, 1993, pp. 527-548.

[9]    Klement, H.D. (1997): Manuals of MADYN, Version 4.2. Program System for Machine Dynamics.

[10]   Muszynska, A. (1989): Rotor-to-stationary element rub-related vibration phenomena in rotating machinery - literature survey. *Shock and Vibration Digest*, March 1989

[11]   Newkirk, Burt L. (1926): Shaft Rubbing. Relative Freedom of Rotor Shafts from sensitiveness to rubbing Contact When Running Above Their Critical Speeds. *Mechanical Engineering*, Vol. 48, No. 8, pp. 830-832, 1926

[12]   Schmied, J. (1987): Spiral Vibrations of Rotors. *Proc. 11th Biennial ASME Design Engineering Div. Conf., Vib. Noise*, DE-Vol. 2 "Rotating Machinery Dynamics", ASME H0400B, 1987, Boston MA, pp. 449-456